Electronic Supplementary Information

ZnO nanoparticle preparation route influences surface reactivity, dissolution and cytotoxicity

Catherine B. Anders,[a] Josh E. Eixenberger,[a] Nevil A. Franco,[b] Rebecca J. Hermann,[c] Katherine D. Rainey,[b] Jordan J. Chess,[d] Alex Punnoose,[b] and Denise G. Wingett *[ac]

[a]Biomolecular Sciences Graduate Programs, Boise State University, Boise, ID 83725
[b] Department of Physics, Boise State University, Boise, ID 83725
[c]Department of Biological Sciences, Boise State University, Boise, ID 83725
[d] Department of Physics, University of Oregon, Eugene, OR 97403

*Address correspondence to Denise G. Wingett, email; denisewingett@boisestate.edu

XRD, XPS and TEM images

XRD (Fig. S1(a) and (b)), TEM (Fig. S1(c) through Fig. S1(j)) and XPS (Fig. S2) and were performed to verify the crystal structure, chemical composition, average size and morphology of the NP samples.
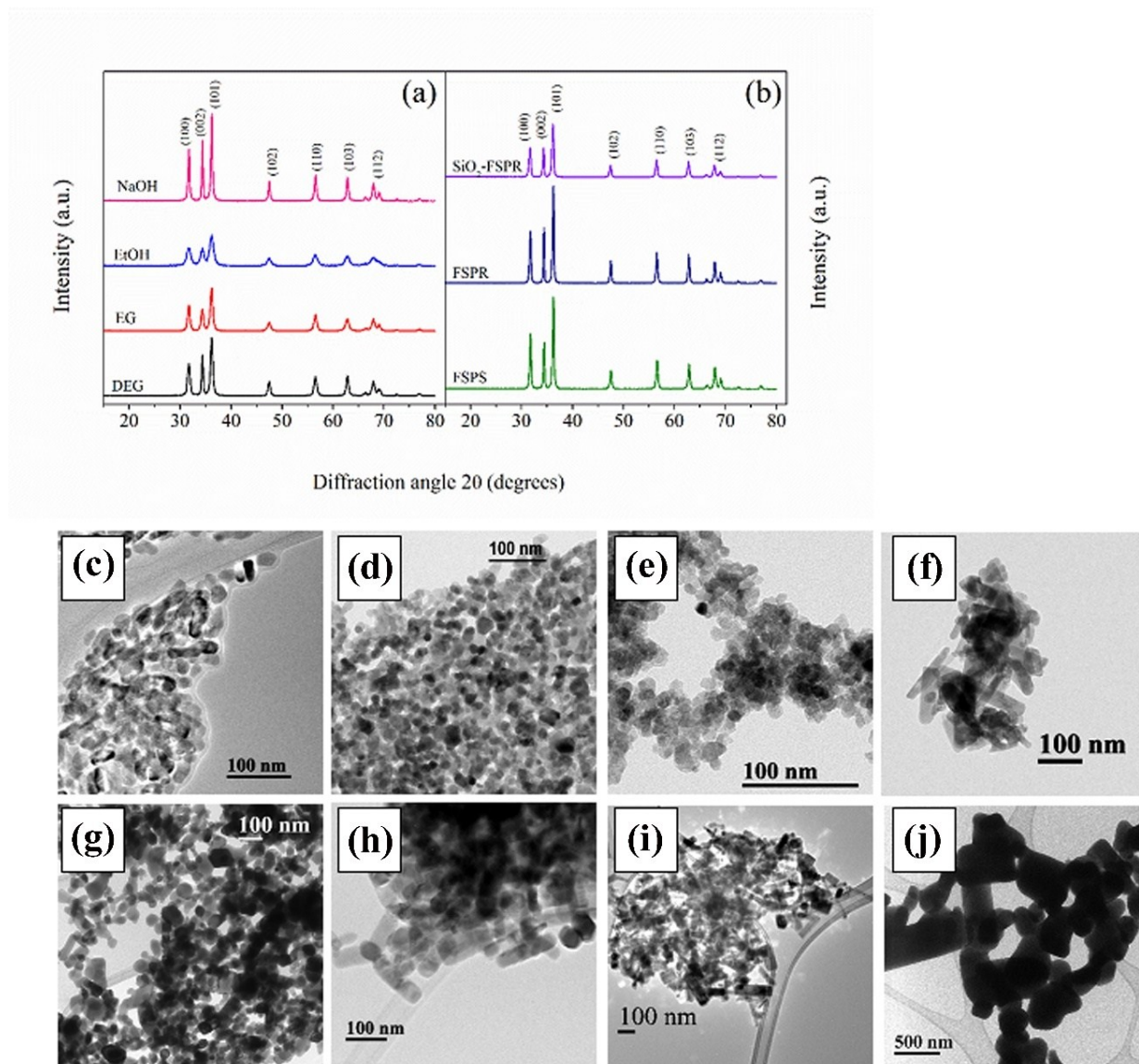

Figure S1 Crystal phase composition, size and morphology characterization for nZnO NPs. XRD spectra for (a) nZnO synthesized through wet chemical synthesis methods and (b) nZnO synthesized through flame spray pyrolysis (FSP) synthesis methods. TEM images for (c) DEG, (d) EG (e) EtOH, (f) NaOH, (g) FSPS, (h) FSPR, (i) SiO_2-FSPR and (j) bulk samples were used to identify morphology and average NP size and distribution.
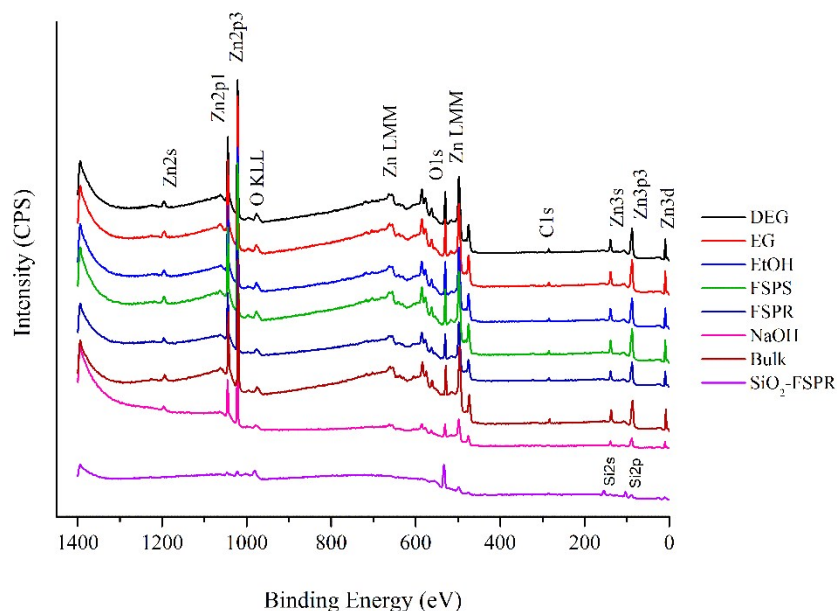
2

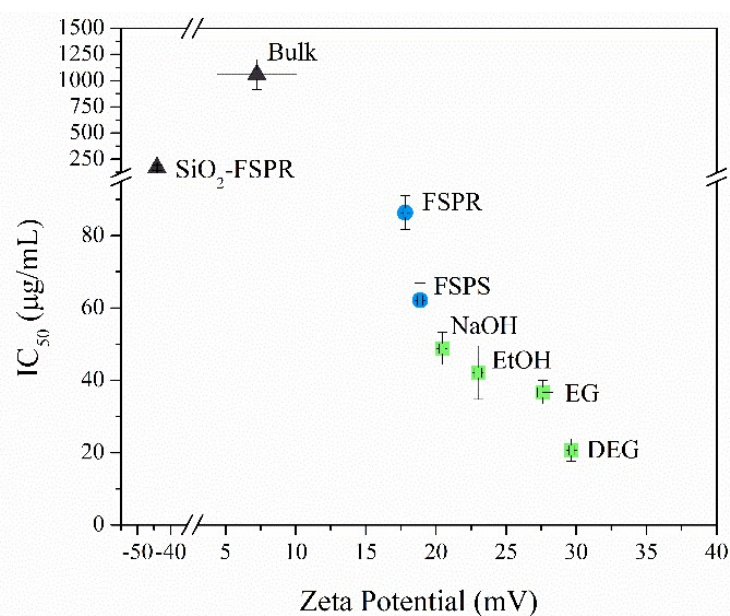**Figure S2**: XPS survey scans for all tested powder samples

Figure S3 IC_{50} (µg/mL) values plotted as a function of the nZnO zeta potential (mV) in aqueous conditions depicting the linear correlation between the two measures variables for wet chemical and FSP synthesized nZnO.

Dissolution kinetics for nanopure water stock solutions

Prior to conducting experiments with cells, we first investigated the kinetic behavior of the panel of nZnO formulations in nanopure water at concentrations identical to the NP stock solutions used in biological assays. Nanopure water dispersions containing 486 µg/mL of each ZnO formulation were prepared and stirred continuously at room temperature for a total of

3

24 hours. At several timepoints, individual aliquots were extracted and prepared for analysis with ICP-MS. The results of this analysis can be seen in Fig. S4. All the samples exhibit similar kinetic behavior throughout most of the experimental time frame. The kinetic pattern generally suggests that the dissolution rate of the NPs is faster from 0.5 to 6 hours and then decreases gradually as the process approaches a dynamic equilibrium [1]. Additionally, this data directly correlates with the measured hydrodynamic sizes of the NP agglomerates in water ($R^2 = 0.88$) validating experimental evidence for the dependence of measured Zn^{2+} concentration on hydrodynamic size [1]. While these results cannot be used to make inferences as to dissolution kinetics of the nZnO under biological assay conditions, these results confirm that at early time points, dissolution of all nZnO samples demonstrate similar kinetic behavior.
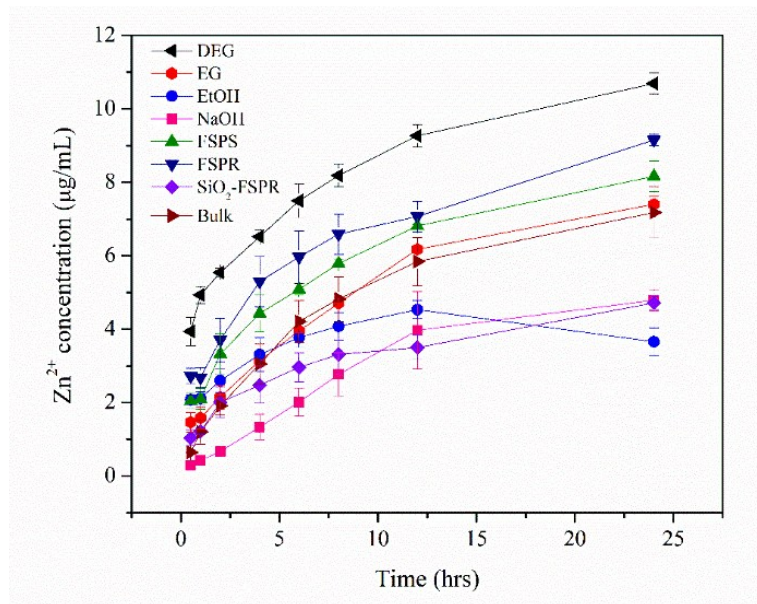

Figure S4: Dissolution kinetics for nanopure water dispersions for all tested formulations

FTIR and FTIR Peak Deconvolution

For this assay, the evaluated samples were incubated in RPMI-based cellular media at a concentration of 32.4 µg/mL and sampled at 4 and 24 hours. Post incubation, the resulting precipitate was isolated and dried overnight. Figure S5 illustrates the vibrational modes present for all samples at 4- and 24-hours. The graphs in Fig. S6 represent the deconvolution of the broad ZnO band present at approximately 350-700 cm^{-1} for all samples at the 24-hour time point. To eliminate zinc phosphate peak overlap with zinc oxide normal modes (Table S1), only those peaks identified below 500 cm^{-1} were included in the ratio of crystalline ZnO to phosphate (ZnO/PO_4^{3-}) calculations. Likewise, only the integrated area of the broad phosphate band at 1031 cm^{-1} was considered in the ratio to eliminate any interference from ZnO in the phosphate determinations.
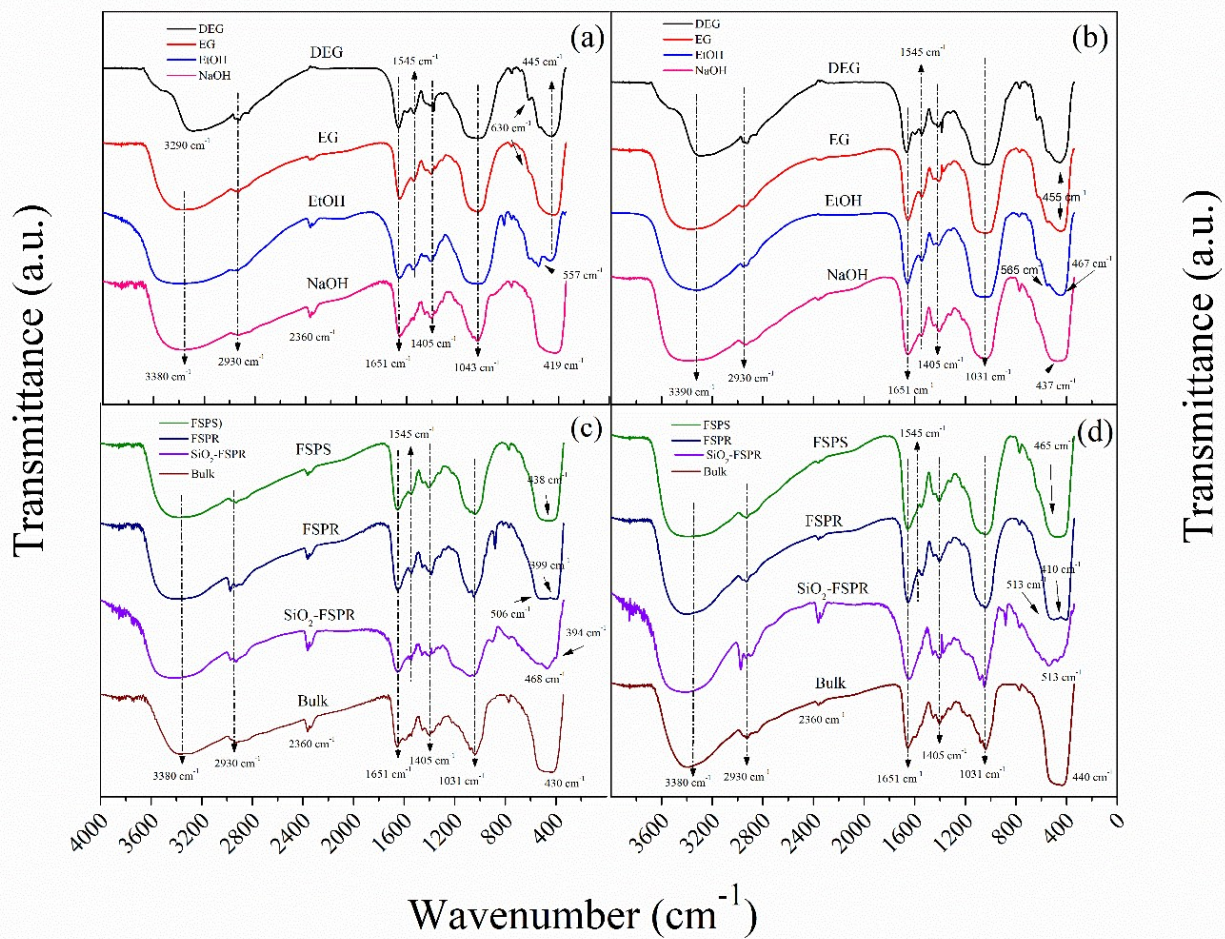
Figure S5 FTIR spectra obtained for the amorphous precipitate material retained at the 4-hour [(a) and (c)] and 24-hour [(b) and (d)] time points. Samples were introduced to cellular media at a concentration of 32 µg/mL and incubated for the indicated time points. After incubation, the dispersions were centrifuged and the precipitate retained and dried overnight at 60 °C.
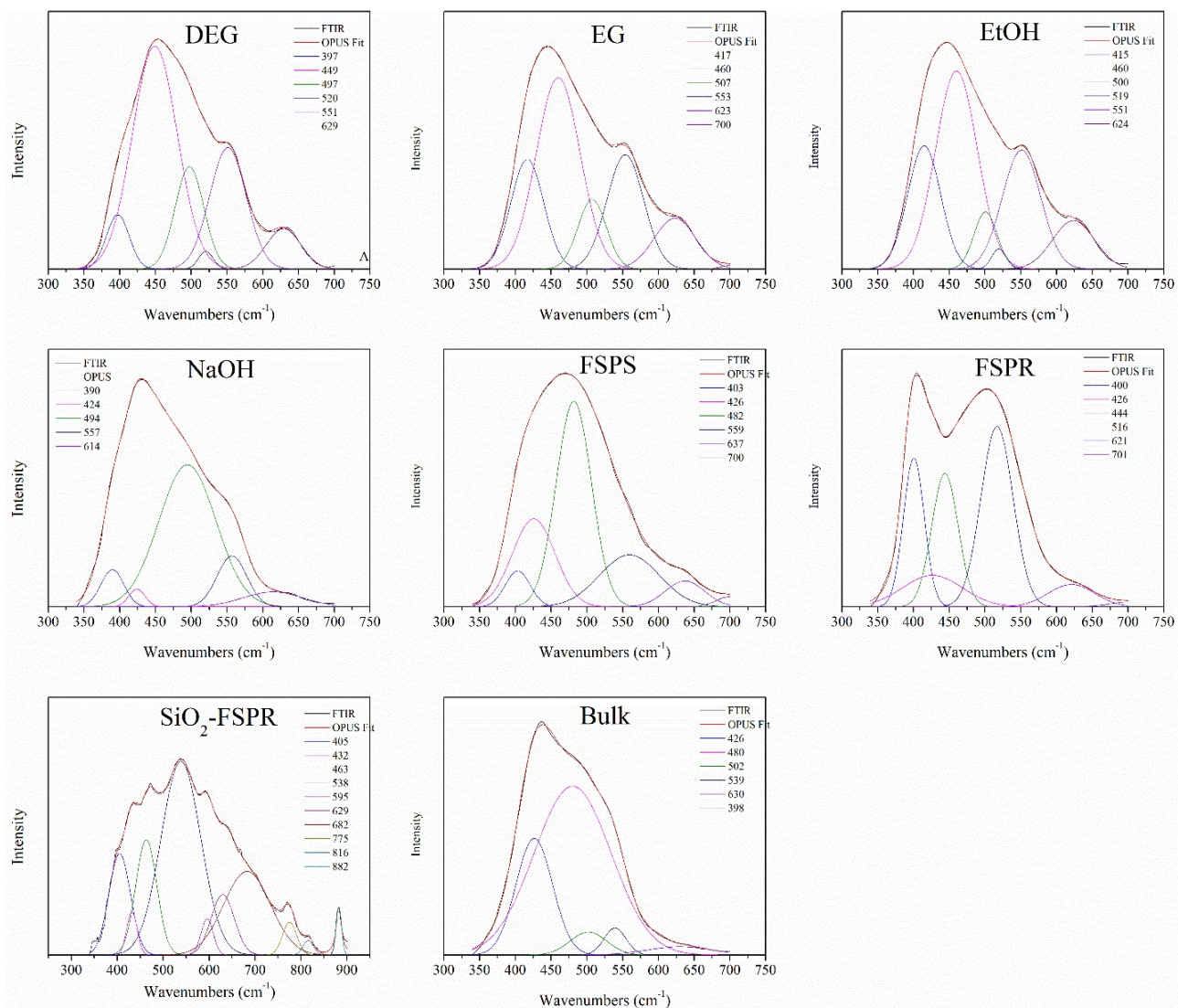
Figure S6 **F**TIR peak deconvolution results for all powdered samples post incubation in cellular media for 24 hours. Each graph is labeled with the sample name with legend numbers corresponding to the peak position (in nm) for each identified peak during the deconvolution process.

XPS spectra of samples in cellular media

XPS was used to confirm the chemical compostion for all samples post incubation in cellular media for 4 and 24 hours (Fig. S3.7). Survey spectra illustrated the presence of zinc, oxygen, nitrogen, carbon and phosphorous in all samples. The SiO$_2$-FSPR sample also contains silica as expected.
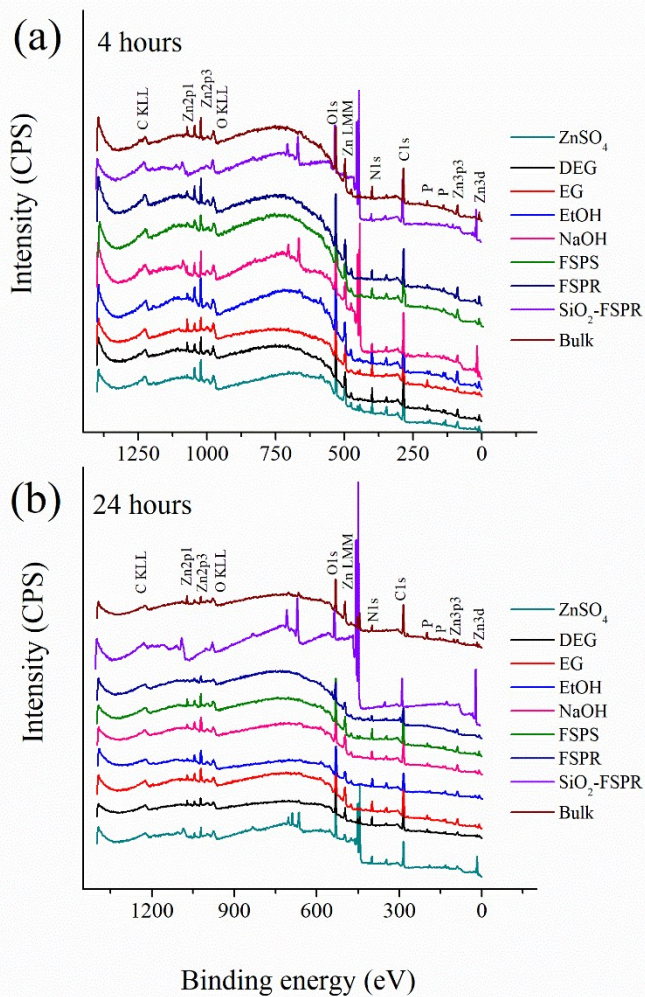
Figure S7: XPS survey scans for all tested samples incubated in cellular media for (a) 4 hours and (b) 24 hours.

Table S1: Identified FTIR peaks for the 24-hour precipitate analysis after deconvolution of the broad ZnO band (350-750 cm^{-1}) including the possible peak assignment and reference

DEG	EG	EtOH	NaOH	FSPS	FSPR	SiO$_2$-FSPR	Bulk	Peak Assignment	Reference
397			390	403	400	405	398	A1(TO)	[2-4]
	417	415	424	426	426	432	426	E1(TO)	[2-7]
449					444			E2 high (Raman)	[3,4,7]
	460	460		482		463	480	Lower surface phonon	[5,7]
497		500	494					Zn-O vibrational mode	[8-12]
520	507	519			516		502	v_4 phosphate mode	[13]
551	553	551	557	559		538	539	v_4 phosphate mode	[13]
						595		v_4 phosphate mode	[13]
629	623	624	614	637	621	629	630	v_4 phosphate mode	[13]
	700			700	701			C-H bending	
						682		Si-H	[14]
						775		O-C rocking	[15]
						816		Si-O-Si bending	[16]
						882		Si$_2$O$_3$	[17,18]

TEM

The following (Fig. S8 through Fig. S15) represent low and high resolution TEM images obtained for the samples described above in the FTIR section. Low resolution images revealed that large nZnO agglomerates (darker areas) were surrounded by an organic matrix. The higher resolution scans provided confirmation that the darker regions of the TEM images were composed of primarily crystalline ZnO due to the presence of observed lattice fringes representing the individual planes of the ordered ZnO.
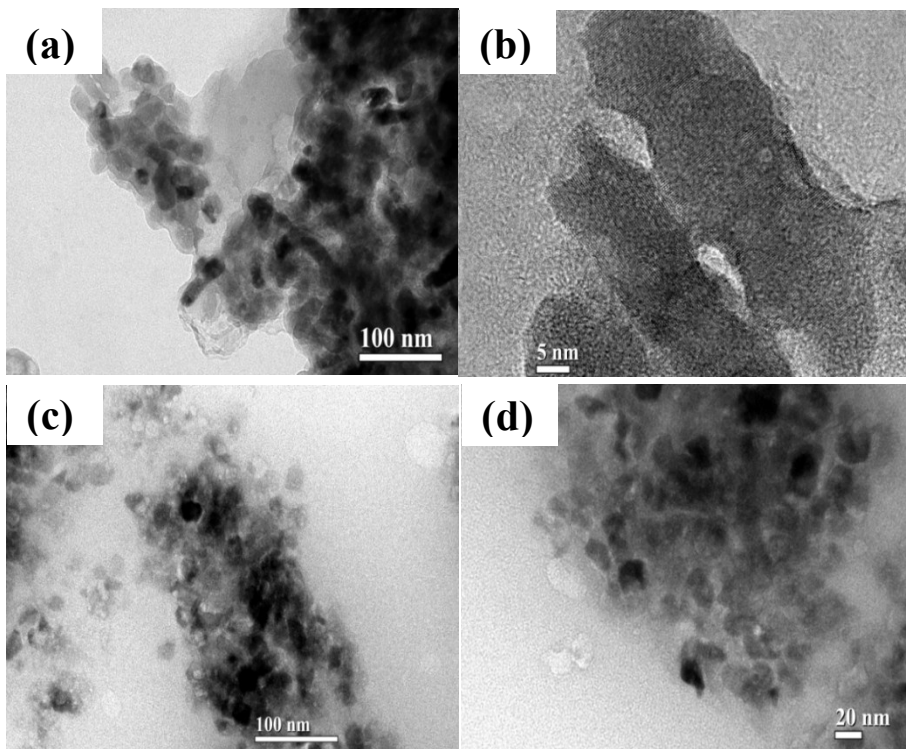
Figure S8: Low (a) and (c) and high (b) and (d) resolution TEM images for the DEG sample precipitates isolated from RPMI-based cellular media at (a) and (b) 4-hour and (c) and (d) 24-hour time points.
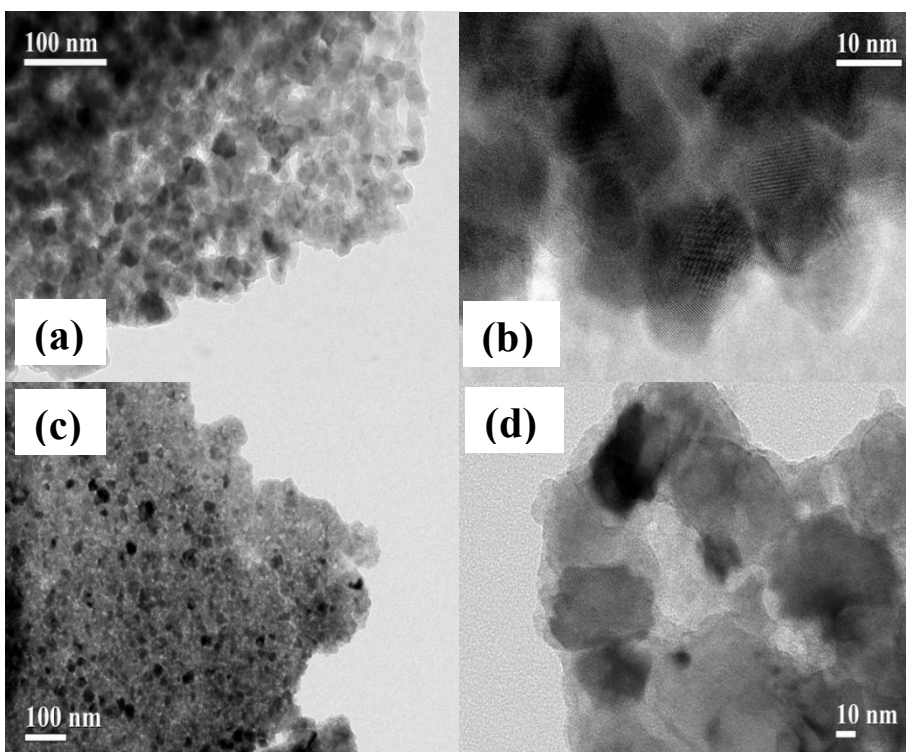

Figure S9: Low (a) and (c) and high (b) and (d) resolution TEM images for the EG sample precipitates isolated from RPMI-based cellular media at (a) and (b) 4-hour and (c) and (d) 24-hour time points.
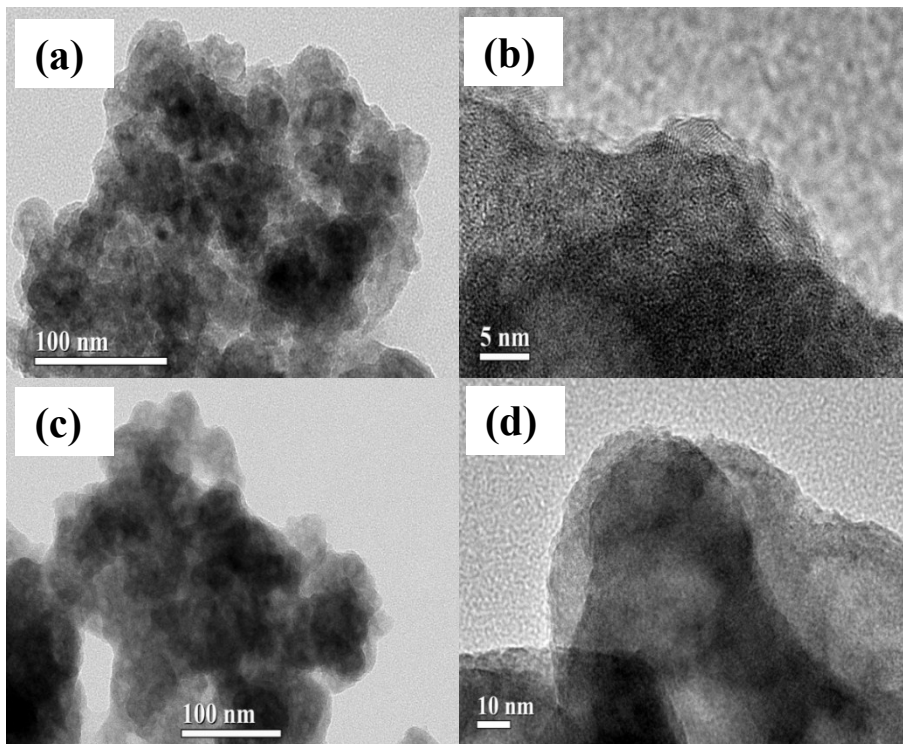
Figure S10: Low (a) and (c) and high (b) and (d) resolution TEM images for the EtOH sample precipitates isolated from RPMI-based cellular media at (a) and (b) 4-hour and (c) and (d) 24-hour time points.
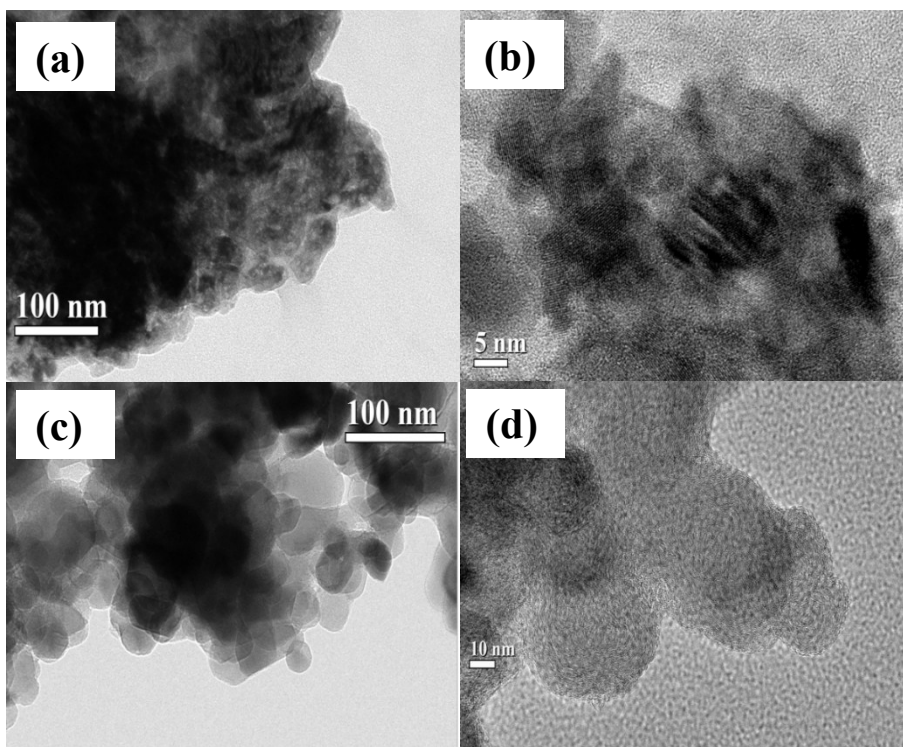

Figure S11: Low (a) and (c) and high (b) and (d) resolution TEM images for the NaOH sample precipitates isolated from RPMI-based cellular media at (a) and (b) 4-hour and (c) and (d) 24-hour time points.
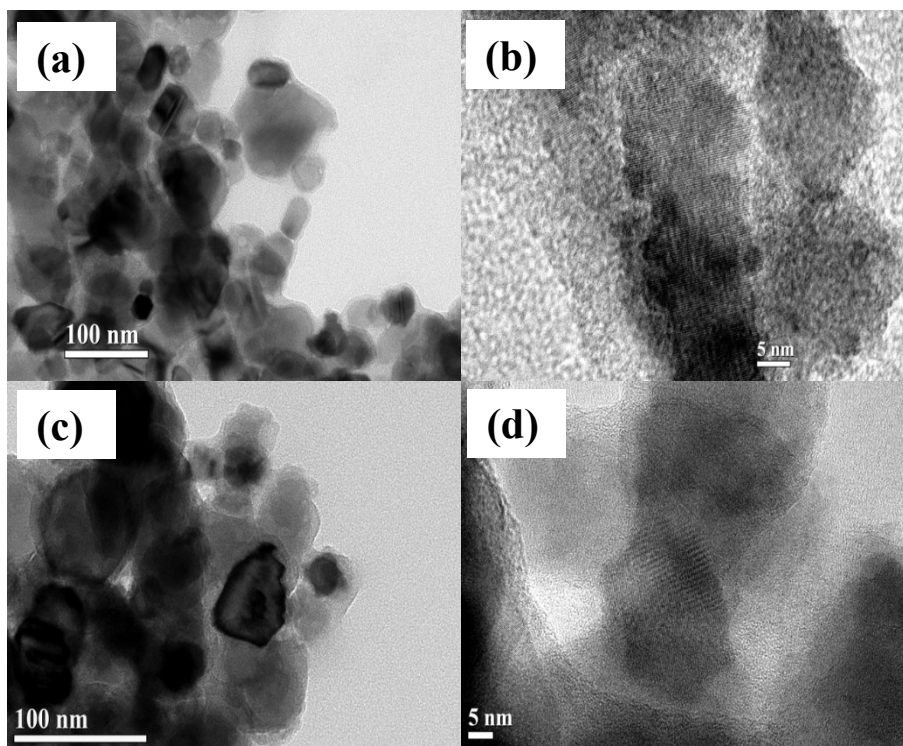
Figure S12: Low (a) and (c) and high (b) and (d) resolution TEM images for the FSPS sample precipitates isolated from RPMI-based cellular media at (a) and (b) 4-hour and (c) and (d) 24-hour time points.

Figure S13: Low (a) and (c) and high (b) and (d) resolution TEM images for the FSPR sample precipitates isolated from RPMI-based cellular media at (a) and (b) 4-hour and (c) and (d) 24-hour time points.
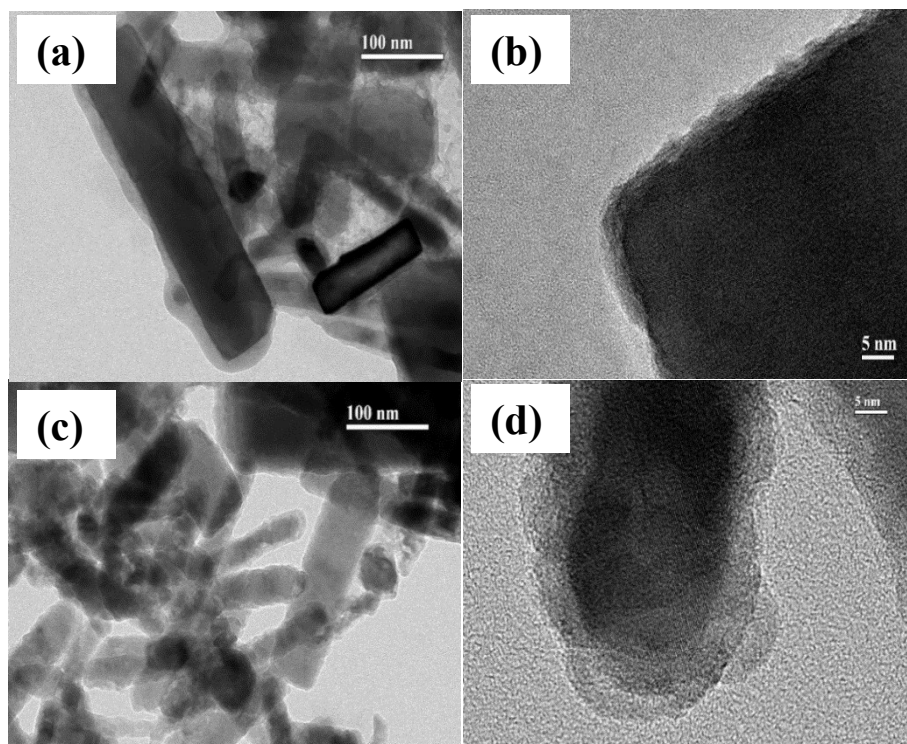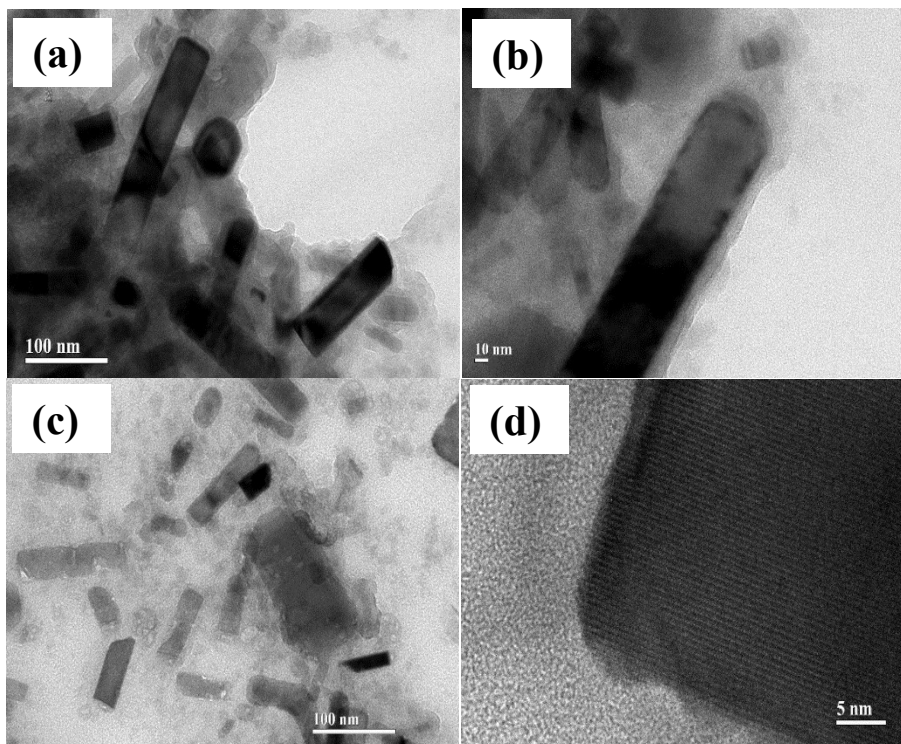
Figure S14: Low (a) and (c) and high (b) and (d) resolution TEM images for the SiO_2 – FSPR sample precipitates isolated from RPMI-based cellular media at (a) and (b) 4-hour and (c) and (d) 24-hour time points.
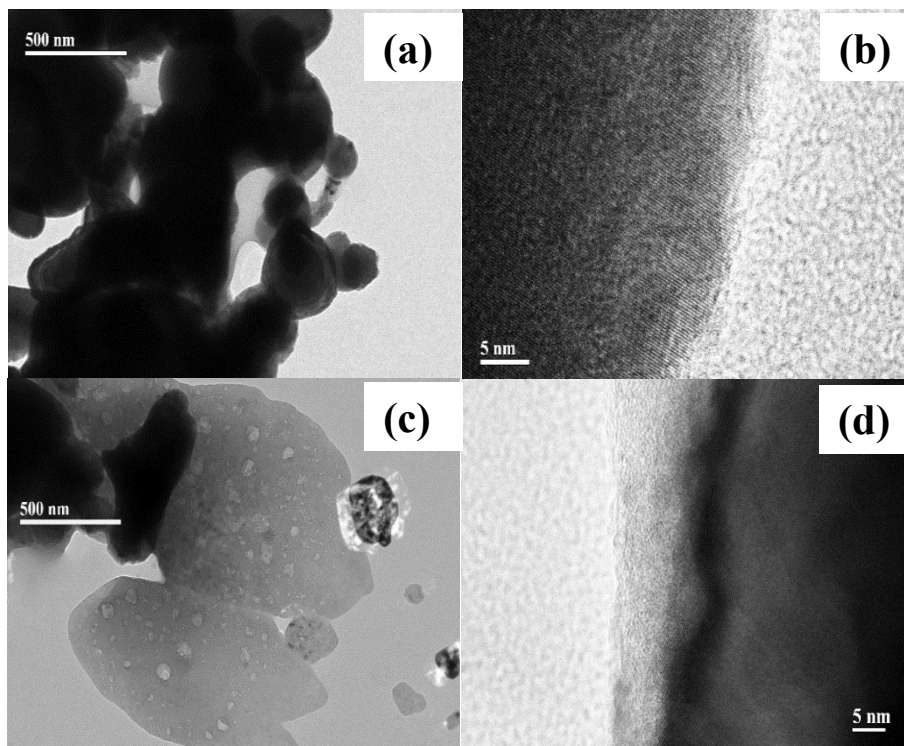

Figure S15: Low (a) and (c) and high (b) and (d) resolution TEM images for the Bulk sample precipitates isolated from RPMI-based cellular Prin media at (a) and (b) 4-hour and (c) and (d) 24-hour time points.

12

Table S2 describes the results of the linear contrast model predictions for Jurkat cells IC_{50} as a function of PC1 and PC2.

Table S2: Linear regression model for IC_{50} as a linear function of PC1 and PC2.

Term	Estimate (S.E.)[2]
Intercept	-4.15 (0.11)
PC1	-1.48 (0.18)
PC2	1.11 (0.17)

[1]**Overall model for IC_{50} as a linear function of PC1 and PC2 is statistically significant ($F_{2, 21}$ = 39.91, p < 0.0001) with 24 observations and is presented as:**

$$Ln(Jurkat\ IC_{50}) = 4.15 - 1.48(PC1) + 1.11(PC2)$$

[2]**All statistically significant at p < 0.0001**

References

1. C. A. David, J. Galceran, C. Rey-Castro, J. Puy, E. Companys, J. Salvador, J. Monné, R. Wallace and A. Vakourov, *The Journal of Physical Chemistry C*, 2012, **116**, 11758-11767.
2. F. Decremps, J. Pellicer-Porres, A. M. Saitta, J. C. Chervin and A. Polian, *Physical Review B*, 2002, **65**.
3. S. Y. Gao, H. J. Zhang, X. M. Wang, R. P. Deng, D. H. Sun and G. L. Zheng, *J. Phys. Chem. B*, 2006, **110**, 15847-15852.
4. R. P. Wang, G. Xu and P. Jin, *Physical Review B*, 2004, **69**.
5. G. Munoz-Hernandez, A. Escobedo-Morales and U. Pal, *Crystal Growth & Design*, 2009, **9**, 297-300.
6. M. A. Verges, A. Mifsud and C. J. Serna, *Journal of the Chemical Society-Faraday Transactions*, 1990, **86**, 959-963.
7. V. Gupta, P. Bhattacharya, Y. I. Yuzuk, K. Sreenivas and R. S. Katiyar, *Journal of Crystal Growth*, 2006, **287**, 39-43.
8. M. M. H. Farooqi and R. K. Srivastava, *Journal of Alloys and Compounds*, 2017, **691**, 275-286.
9. Y. He, W. B. Sang, J. Wang, R. F. Wu and J. H. Min, *Journal of Nanoparticle Research*, 2005, **7**, 307-311.
10. M. F. Khan, A. H. Ansari, M. Hameedullah, E. Ahmad, F. M. Husain, Q. Zia, U. Baig, M. R. Zaheer, M. M. Alam, A. M. Khan, Z. A. AlOthman, I. Ahmad, G. M. Ashraf and G. Aliev, *Scientific Reports*, 2016, **6**, 11

11. A. Sahai and N. Goswami, *Physica E-Low-Dimensional Systems & Nanostructures*, 2014, **58**, 130-137.
12. G. Vijayaprasath, R. Murugan, Y. Hayakawa and G. Ravi, *Journal of Luminescence*, 2016, **178**, 375-383.
13. O. Pawlig and R. Trettin, *Materials Research Bulletin*, 1999, **34**, 1959-1966.
14. C. Tsai, K. H. Li, J. Sarathy, S. Shih, J. C. Campbell, B. K. Hance and J. M. White, *Applied Physics Letters*, 1991, **59**, 2814-2816.
15. S. E. Babayan, J. Y. Jeong, V. J. Tu, J. Park, G. S. Selwyn and R. F. Hicks, *Plasma Sources Science and Technology*, 1998, **7**, 286.
16. H.-L. Xia and F.-Q. Tang, *The Journal of Physical Chemistry B*, 2003, **107**, 9175-9178.
17. I. W. Boyd and J. I. B. Wilson, *Journal of Applied Physics*, 1982, **53**, 4166-4172.
18. M. Nakamura, Y. Mochizuki, K. Usami, Y. Itoh and T. Nozaki, *Solid State Communications*, 1984, **50**, 1079-1081.